# Experimental and Analytical Investigation on In-Plane Behavior of URM Flanged Walls

*M. Khanmohammadi[1], H. Behnam[2], and M.S. Marefat[3]*

1. Assistant Professor, College of Engineering, University of Tehran, Iran,
* Corresponding Author; email: mkhan@ut.ac.ir
2, MSc. in Earthquake Engineering, College of Engineering, University of Tehran, Iran,
3. Professor, College of Engineering, University of Tehran, Iran

## ABSTRACT

*The shape of most of the wall sections in existing unreinforced masonry (URM) structures have L, T, and H shapes, instead of rectangle. Limited research on the effect of return wall (flange) on their seismic behavior has been reported in the literature. The primary aim of this study is to develop a deeper understanding of in-plane response of URM walls with emphasis on return walls. The URM shear walls represent existing masonry structures with poor shear strength. An Experimental program has been conducted on four specimens with aspect ratios of 0.5 and 0.7. Two specimens designed with flanges and, for comparison, another two specimens designed without flanges. All specimens tested under constant axial force corresponding to typical 3-story buildings, and cyclic reversal displacement control loading was applied in horizontal direction. Predicted shear strength based on FEMA-356 has been compared with experimental results. An analytical model has been proposed to predict lateral response of flanged URM walls. The results emphasize on the effect of flanges when seismic assessment of non-rectangular section URM walls is considered.*

**Keywords:**
Unreinforced Masonry;
Return wall (flange);
Shear strength;
Experimental;
Analytical model

## 1. Introduction

There are many unreinforced masonry (*URM*) buildings in earthquake-prone regions worldwide. Reports show that more than 70 percent of residential buildings in Iran are of this type and most of them are vulnerable to earthquake. To evaluate seismic capacity of these buildings, numerous studies have been conducted in different countries. Extensive experimental studies have been conducted to investigate the nonlinear behavior of rectangular section unreinforced masonry (*URM*) walls [1-7]. These studies revealed that wall aspect ratio (the wall height-to-length ratio), vertical stress, and masonry material properties are the primary parameters affecting the behavior of an *URM* wall. Based on experimental result, Guidelines such as those of *FEMA* 356 [8] have been developed to determine modes of failure of walls with different material properties, axial load and boundary conditions.

But in contrast to the idealized rectangular section *URM* walls, walls in a *URM* building often do not have a rectangular section, such as walls at the corner of the building or those adjacent to interior walls. Research has been previously presented on in-plane *URM* wall response, but it has been identified in the literature [9-15] that codified equations for assessing the strength and displacement capacity of walls are overly conservative, particularly when assessing *URM* walls with flanges (return walls) at either or both ends. Consequently, the objective of this research was to investigate the response of flanged *URM* walls, in the context of previous research considering failure modes, and to determine strength and displacement limits. Yi et al [11] noted that previous experimental research at the structural level highlighted the effects of transverse walls (flanges) on the response of in-plane walls and

indicated the potential for flanges to influence wall failure modes and maximum strength. They also noted that no experimental data were available which specifically investigate flanged *URM* walls. Experiments conducted by Moon et al [6] and Yi [7] suggested that substantial flange participation was observed for in-plane walls in each loading direction in a full-scale *URM* test structure. Flanges were defined as the portion of the out-of-plane wall that participates with the in-plane wall to resist lateral loads [16]. Following full scale testing of a two-storey *URM* building where significant flange participation was observed, they developed an analytical model to investigate the effects of flanges on the behavior of individual non-rectangular *L* section *URM* walls [6, 17]. Russell and Ingham [14] and Russell [15] noted that the existing simplified predictive techniques of *FEMA* 356 [8] do not accurately take into account the effects of boundary conditions, in particular the influence of perpendicular walls, to the failure mode of in-plane loaded walls. Experiments conducted by them showed walls with flanges can sustain higher levels of lateral force than walls without flanges, when taking into account the wall aspect ratio and axial load.

It is important to note that a lot of existing buildings in Iran are unreinforced masonry. Almost all existing *URM* buildings, due to lack of proper seismic details and weak shear strength, are expected to perform poor in earthquake. On the other hand, detailed seismic evaluations of existing buildings are necessary to make decision on rehabilitation strategy. A well detailed seismic assessment of existing buildings is characterized which seismic properties in building behavior need to be improved or enhanced. The current research was conducted with the primary aim of developing a deeper understanding of the response of *URM* walls, with emphasis on in-plane behavior of flanged *URM* walls. In order to better understand the flange effects in masonry building behavior, knowledge of the flange effects in each individual wall is necessary. However, little research in consistent with our practice, either experimental or analytical, has been carried out to clarify flange effect on the behavior of in-plane walls.

This study is focused on seismic evaluation of existing *URM* shear wall with weak shear strength and flanged section in both end sides. The influence of flanges (return walls) on the in-plane lateral behavior of unreinforced masonry (*URM*) walls with weak shear strength is reported. Predicted shear strength determined based on *FEMA* 356 [8] is compared with experimental results, including shear strength and deformation drift capacity. An analytical model is proposed to predict lateral response of flanged *URM* walls.

## 2. Experimental Programme

Specifications of wall specimens selected based on existing *URM* buildings in Iran. The scale of specimens and brick units were one half, with clay bricks of dimensions of $100mm \times 30mm \times 50mm$. The bed joints designed $5mm$ thick, and the maximum sand aggregate size is $3mm$. Two specimens were designed with flanges of *H* and *U* shapes, and for comparison, two additional specimens were designed without flanges. Details of the walls are shown in Table (1) and Figure (1).

**Table 1.** Wall specifications.

| Wall | Shape | $t_w$ mm | $h$ mm | $l$ mm | $t_f$ mm | $b$ mm | $f'_m$ MPa |
|---|---|---|---|---|---|---|---|
| URMW-1 | Rectangular | 160 | 1350 | 2700 | - | - | 3.21 |
| FIURMW-19 | H | 160 | 1350 | 2820 | 160 | 1560 | 3.21 |
| URMW-2 | Rectangular | 110 | 1350 | 1900 | - | - | 3.21 |
| FUURMW-18 | U | 110 | 1350 | 1930 | 110 | 800 | 3.21 |

The effective length of flanges can be determined according to *MSJC* 2008, see Figure (2), or *EURO CODE*6, see Figure (3), but in this study the definition from *UC*6 is utilized. According to *UC*6, a limited portion of an intersecting wall can act as a flange to a shear wall. The flanges were constructed with the thickness equal to wall thickness inside the plane and simultaneously to construction of this wall. The *H*-shaped Wall (*FIURMW*-19) had flanges at both ends with a length of $700mm$ on either side of the in-plane wall with a total flange length of $1560mm$. Wall *FUURMW*-18 (*U*-shaped wall) had flanges at both ends, but on a single side only, and the flanges had a length of $800mm$ on the side of the in-plane wall.

A concrete diaphragm was built on top of walls as a rigid floor. The diaphragm was intentionally made stiff, and its purpose was to enable the horizontal force to be distributed (among the joists),

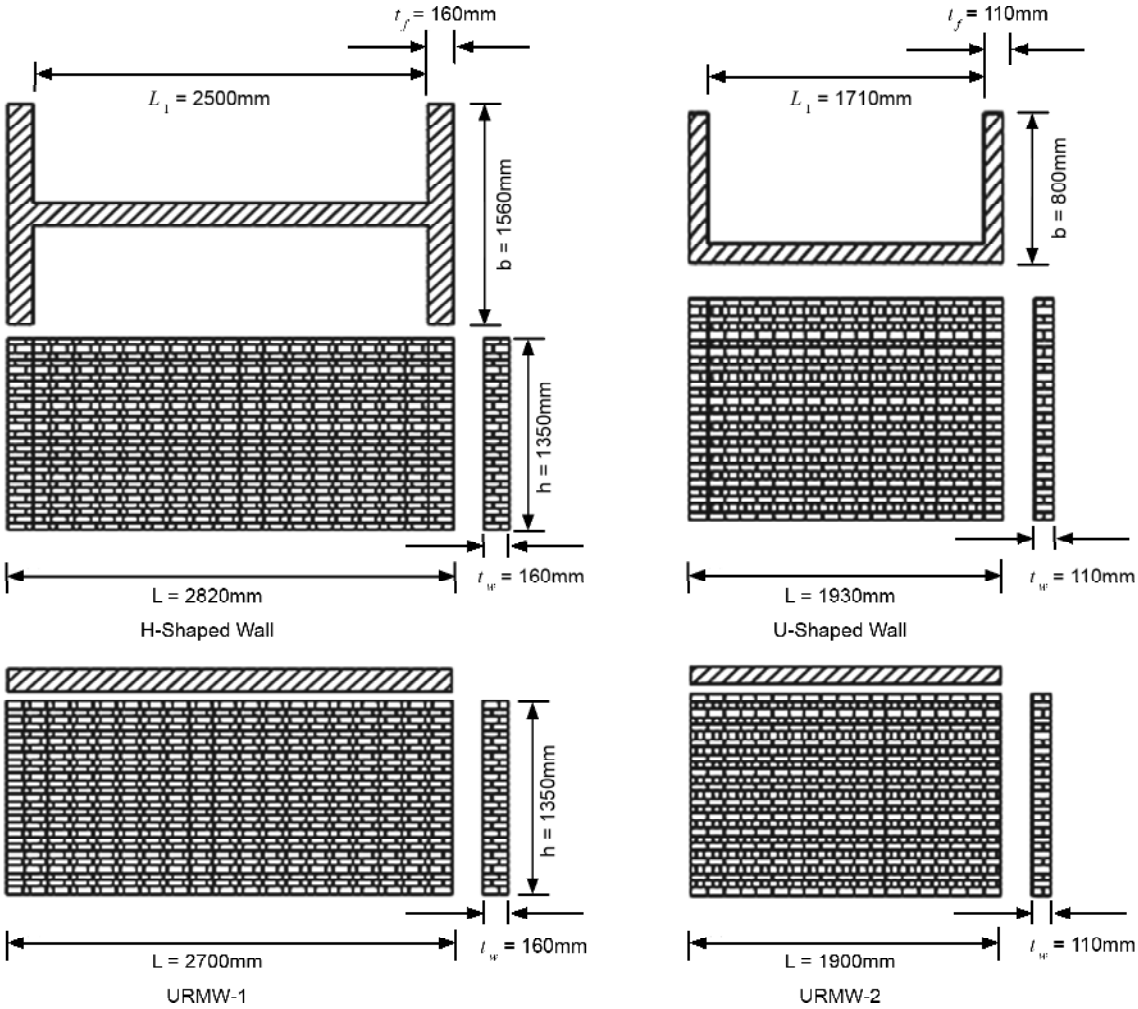


**Figure 1.** Detail of walls.

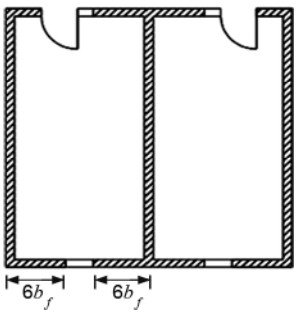


**Figure 2.** Effective flange lengths on plan view of general URM building (MSJC 2008) [18].

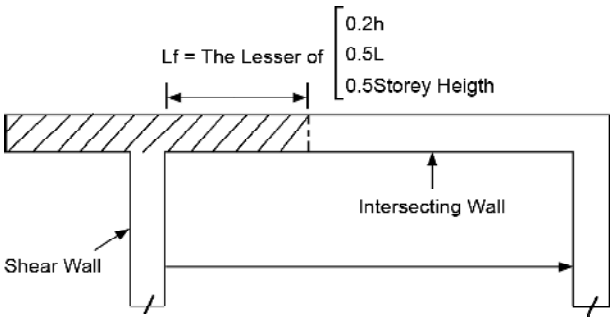


**Figure 3.** Effective flange widths of shear walls (EC6).

instead of being applied at a single point in the top corner of the test wall. The diaphragm was also used to provide a platform for application of axial (gravity) load.

To evaluate the material properties, three tests on mortar, brick, and masonry were carried out, and the results are listed in Table (2). A weak mortar mix (1:6.5 cement /sand by volume) was selected to simulate decayed mortar in old *URM* structures. Standard Portland cement (type 2) and river sand were used in the mortar. All material tests were conducted according to *ASTM* standards.

The typical wall setup is shown in Figures (4) to Figure (10). The walls were loaded laterally by means of a hydraulic actuator reacting against the laboratory strong farms. The wall was built directly onto the strong-floor.

A reinforced concrete slab (diaphragm) was

**Table 2.** Material property.

| Parameter | Mortar Compressive Strength ($f_{mc}$) | Brick Compressive Strength ($f_{bc}$) | Masonry Compressive Strength ($f_m$) |
|---|---|---|---|
| **Strength** | 8.1 | 8.7 | 3.24 |
| **Method of Test (ASTM)** | C109/C109M-02 [20] | C67-03a [21] | C1314-03b [22] |

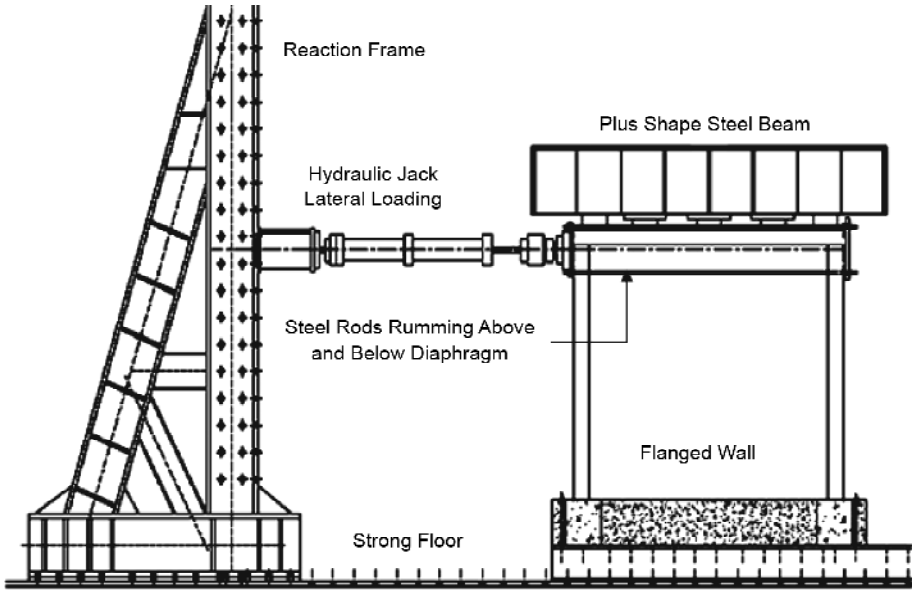


**Figure 4.** Test setup (front view).

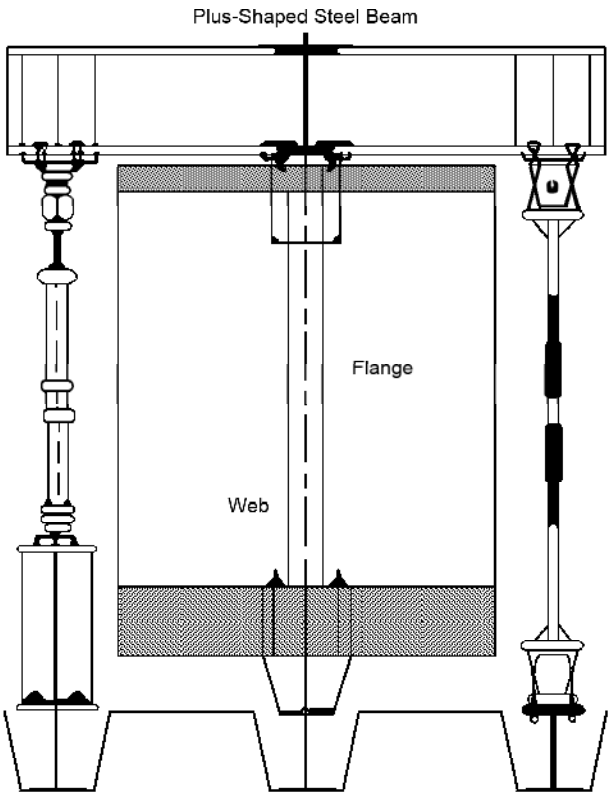


**Figure 5.** Test setup (side view).

built on top of the *H* and *U*-shaped walls. It was intended to uniformly distribute lateral load on top of walls. The lateral loads were transferred through stiff plates that designed to the underside of the diaphragm. The contact surface designed in a way that applied horizontal load was transferred into the wall through slab-wall contact friction and also direct pressure into the top three courses of the wall.

In reference walls (*URMW*-1 and *URMW*-2), a stiff concrete beam is made on top of wall using for lateral loading, which showed good performance during the test. The non-flanged walls have been restrained against out-of-plane failure by a couple of *U*-shaped steel profiles on both ends of the walls.

The flanged walls are restrained against out of plane deformation by a concrete roof at the top of specimens. As a rigid diaphragm, the concrete roof also assists in distribution of lateral load between wall components and flanges. All specimens tested under constant axial force corresponding to axial stress suffered in a typical prototype three-story building. The axial load on *H*-shaped wall and

*URMW*-1 was 44.8*kN*. The axial load on *U*-shaped wall and *URMW*-2 was 21.2*kN*. Lateral load was applied in cyclic reversal pattern under displacement control mode and exerted on centreline of the in-plane wall. The walls are cantilever, i.e. fixed at the base and free at the top. The load pattern of the horizontal actuator is shown in Figure (6). To measure displacements at different locations, 14 linear variable displacement transducers (*LVDT*) for each specimen, have been used.

The used lateral load setup are also employed in other researchers program [23-26].

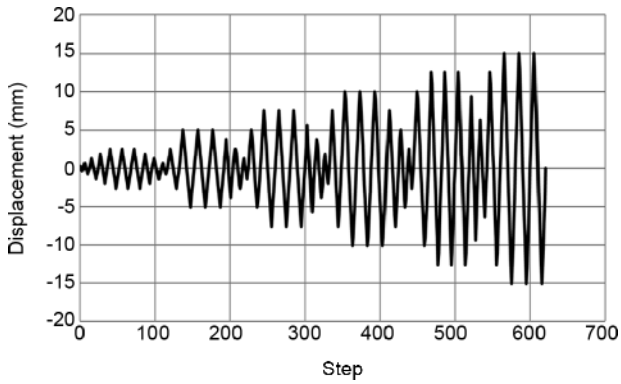


**Figure 6.** Loading protocol.

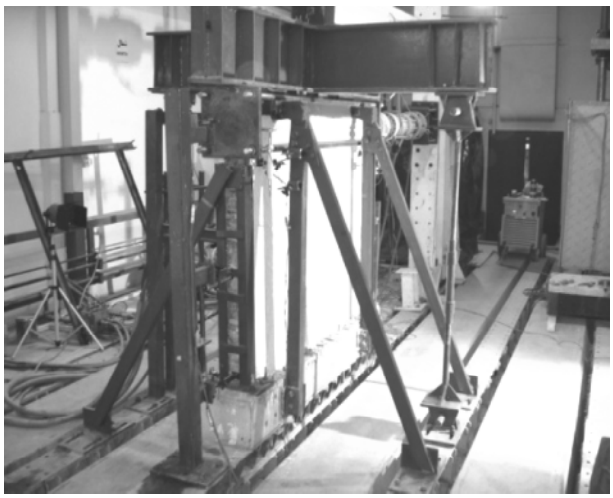

**Figure 7.** URMW-1 wall setup.

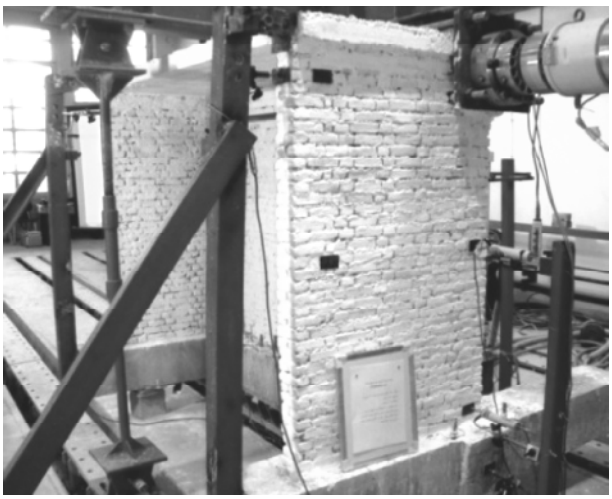

**Figure 9.** U-shaped wall setup.

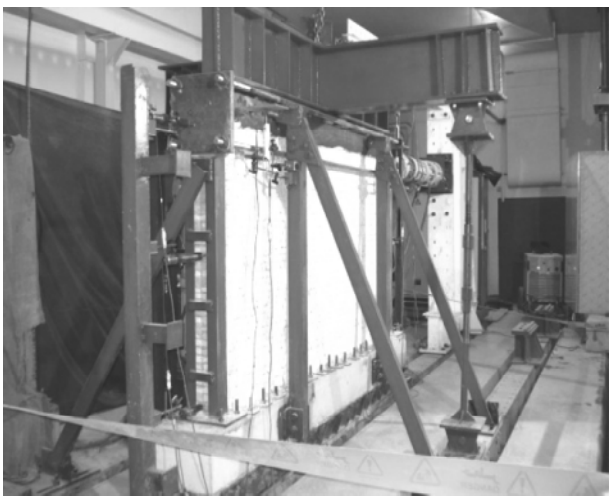

**Figure 8.** URMW-1 wall setup.

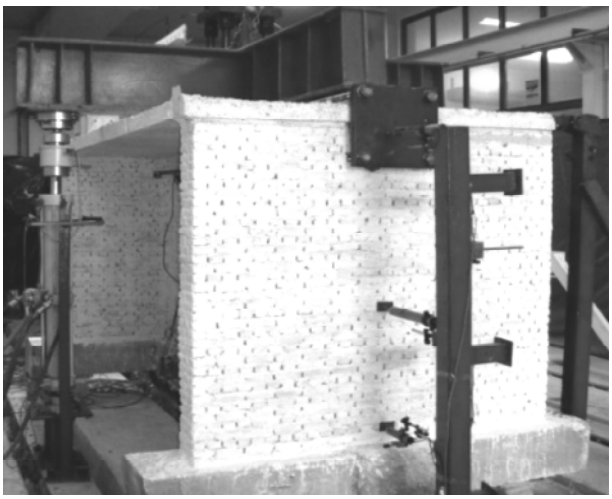

**Figure 10.** H-shaped wall setup.

## 3. Test Observations

Crack pattern and hysteretic behavior of *H*-shaped wall are shown in Figure (11). The specimen suffered considerable damage at a drift of 0.36% where horizontal cracks appeared in the web panel. In addition, inclined cracks formed at web and flange intersection. At drift 0.9%, flanges suffered significant damage in terms of relatively wide vertical cracks parallel to the web, and the cracks extend throughout the flange height.

The crack pattern and hysteretic behavior of reference wall associated with *H*-shaped illustrated in Figure (12). The first cracks initiated at .18% drift ratio. These cracks are located at the bottom of the wall about 300*mm* above foundation. This crack expanded in horizontal direction and continued approximately to 60% of the wall length. At a drift of 0.37%, slide mechanism has been observed and consequently developed.

In the *U*-shaped wall, the cracks appeared in a diagonal tension form. The specimen showed an out-of-plane deformation through the height while it was restrained against out-of-plane deformation at the top slab level. Shear transmission at the middle of wall height caused the web to show out of plane distortion, and this was amplified by the difference between the centre of shear and centre of horizontal loading. In addition, during the tests, wide and deep cracks have been developed in flange edges. The crack pattern and hysteretic behavior of *U*-shaped specimen illustrated in Figure (13). In the reference wall corresponding to *U*-shaped wall, inclined cracks extend towards the diagonal direction in the edges and in the middle of the wall at drift 0.18%, and at drift 0.74%, the diagonal cracks propagate throughout the specimen. Specimen damages at the end of test and lateral load behavior are shown in Figure (14).

Table (3) shows the test results including the maximum lateral load capacity, displacement capacity, and performance of specimen from viewpoints of crack pattern characteristics and limit states.

$V_{max}$ is the maximum recorded lateral force, $d_{v,max}$ and $\theta_{V,max}$ are displacement and drift corresponding to $V_{max}$ respectively, $V_{crack}$ is first observed initiated cracking lateral force, $\theta_{crack}$ is the drift corresponding to $V_{crack}$, and $d_u$ and $\theta_u$ are the lateral

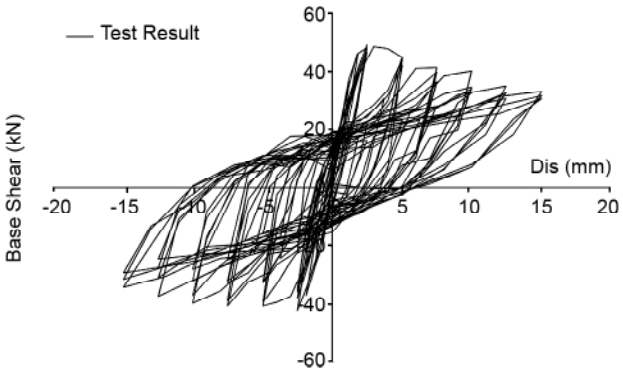


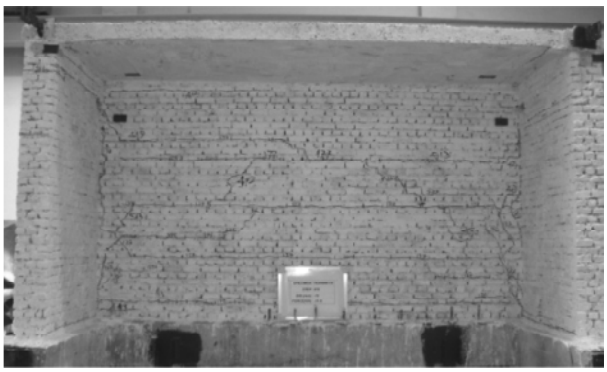

**Figure 11.** Crack pattern and hysteretic behavior of FIURMW-19 (H-shaped).

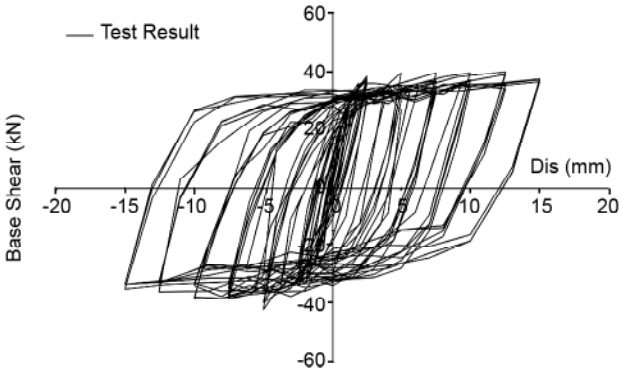


**Figure 12.** Crack pattern and hysteretic behavior of URMW-1.

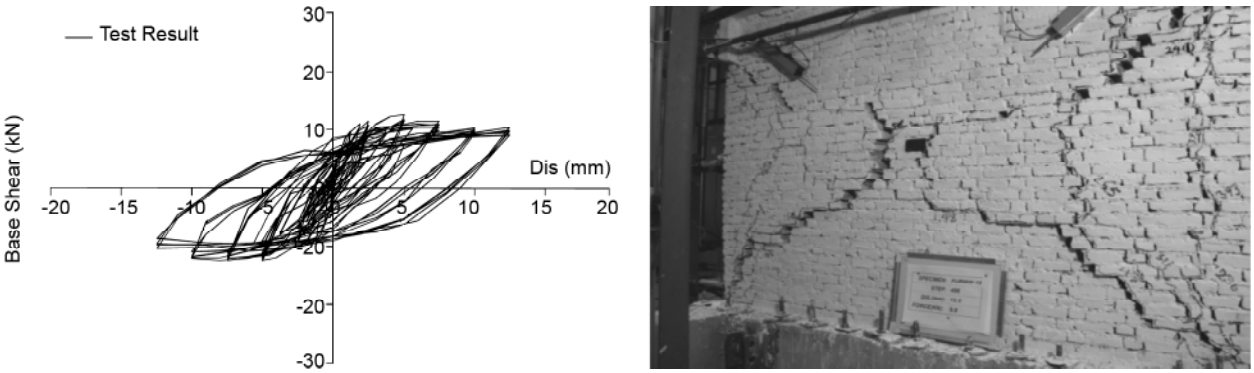


**Figure 13.** Crack pattern and hysteretic behavior of FUURMW-18(U shape).

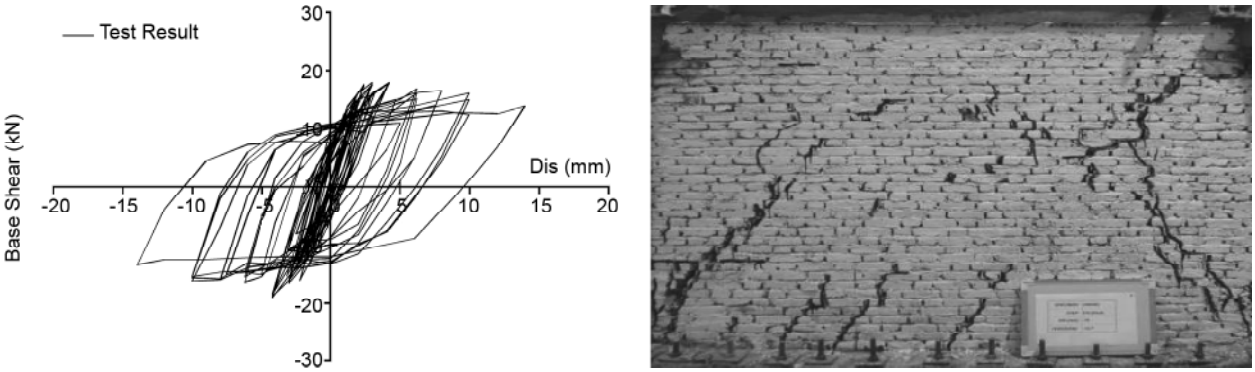


**Figure 14.** Crack pattern and hysteretic behavior of URMW-2.

**Table 3.** Test results.

| Wall | $\sigma_b$ *MPa* | $V_{max}$ *kN* | $d_{V,max}$ *mm* | $\theta_{V,max}$ *%* | $V_{crack}$ *kN* | $\theta_{crack}$ *%* | $d_u$ *mm* | $\theta_u$ *%* | Test Failure Mode |
|---|---|---|---|---|---|---|---|---|---|
| URMW-1 | 0.1 | 41.8 | 5 | 0.37 | 28 | 0.09 | 15 | 1.11 | Slid |
| FUURMW-19 | 0.1 | 47.9 | 2.5 | 0.18 | 46 | 0.13 | 10 | 0.74 | Slid |
| URMW-2 | 0.1 | 18.3 | 3 | 0.22 | 14.9 | 0.13 | 13 | 0.96 | Diagonal Tension |
| FUURMW-18 | 0.1 | 12.4 | 5 | 0.37 | 10 | 0.10 | 13 | 0.96 | Diagonal Tension |

wall displacement and drift corresponding to 80% strength degradation, where $\theta_u = d_u/h_{eff}$.

### *3.1. Out-of-Plane Behavior Observations*

Out-of-plane behavior has been recognized as one of the predominant failure modes in infilled and *URM* walls during the last earthquakes [27-28]. In general, in-plane walls bahvior in a *URM* low-rise structure are considered primary lateral-load resisting components while due to low lateral acceleration in bottom stories out-of-plane behavior is considered secondary. Although out-of-plane behavior is important as noted, the main effort in this research was focused on in-plane behavior. On the other hand, lateral load testing of specimens was impossible in our laboratory. The out-of-plane behavior observations are also reported in the following.

In the *H*-shaped wall with increasing displacement horizontal flexural cracks occurred at a mortar bed joint at top and bottom of the wall and also around the midheight of each transverse wall (flanges). In drift 0.9% the significant damage occurred in flanged walls. In this step, the vertical crack in vicinity of the axis of main wall initiated and spread through height of the wall and separated web-flange intersection. The induced web moments to flange caused poor performance of flanged wall. Masonry crushing did not occur in this test. Pattern of cracks at the end of the test are shown in Figure (15).

In *U*-shaped wall as shown in Figure (16), with increasing displacement, a horizontal crack occurred at a mortar bed joint at top and bottom of the wall. Due to the moment resulting from torsion, deep cracks have been created in flange edges around the height of each transverse wall. In drift 0.9% the significant damage occurred in the out-of-plane walls (flanges). In this step, the vertical crack in vicinity of the axis of main wall spread approximately in total height of the wall and separated transverse wall from web. The suffered damage and crack pattern of *U*-shaped wall was more significant than *H*-shaped wall so that it was concerned the wall failed vertical load caring capacity.

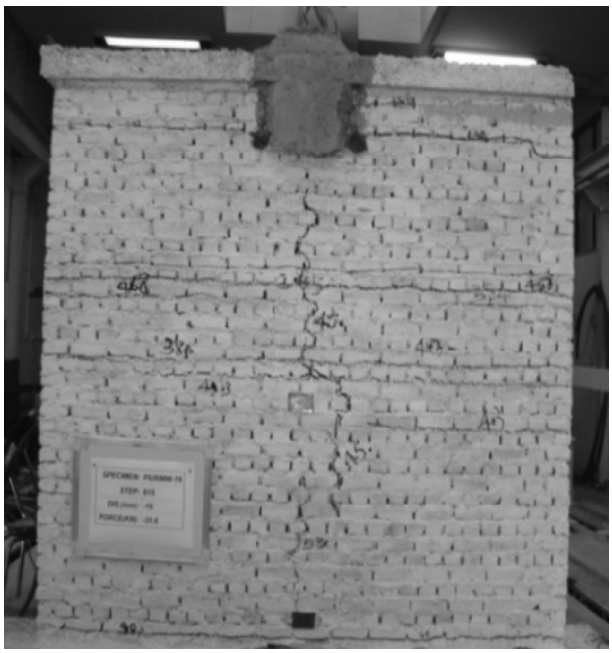

**Figure 15.** Crack pattern on flange side of FIURMW-19 (H-shaped at the end test).

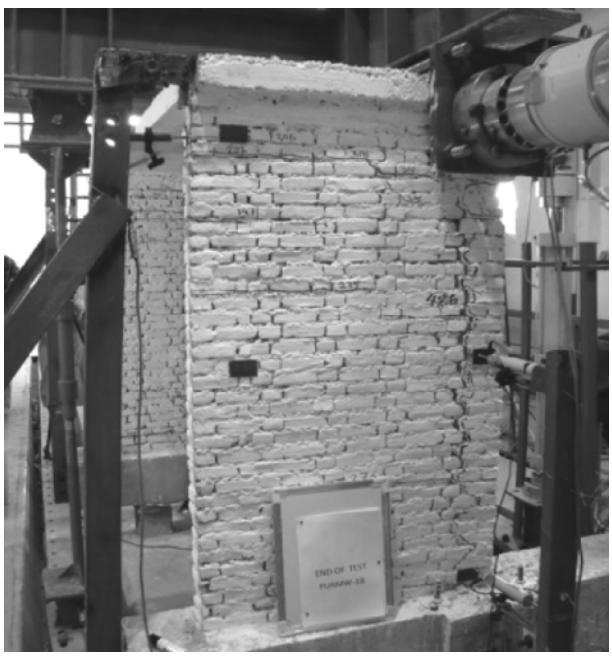

**Figure 16.** Crack pattern on flange side at drift 0.9% of FUURMW-18 (U-shaped wall).

## 4. Comparison of Flanged Walls with Reference Walls

The response and damage of the *H*-shaped wall and the corresponding reference wall are illustrated in Figures (11) and (12), respectively. In addition, maximum strength, initial stiffness, first cracks and failure modes of different specimens are presented in Table (3). It is seen that initial stiffness, first cracking stage, and mode of failure of two specimens are almost the same. The flanged wall shows a greater strength by about 17% while lower deformation capacity by about 50%. It should be noted that the reference wall experiences much more severe damage relative to the flanged wall at a drift ratio of 1%. The location of damage in the reference wall concentrates in the slide joints at the bottom of the wall, but in the flanged wall, the damage has distributed over the height of the wall. This is caused by relatively large sliding of the reference wall while restriction of flanges against sliding for the flanged wall. As a consequence, the hysteresis curve of the reference wall lacks large pinching effect while the flanged wall experiences much higher pinching in the curve.

The response and damage of the *U*-shaped wall and the corresponding reference wall are illustrated in Figures (13) and (14), respectively, and the maximum strength, initial stiffness, first cracks and failure modes of different specimens are presented in Table (3). The flanged wall suffers more than 30% loss of strength which has been caused by out-of-plane torsion of the *U*-shaped wall. But, both walls indicate almost similar initial stiffness, deformation capacity, and mode of failure.

## 5. FEMA 356 Predictions of In-Plane URM Walls Behavior

The results of the tests are compared with predictions from *FEMA*356. As per *FEMA*356, strength of the *URM* walls without flanges is given by the minimum of the following Eqs. (1) to (4):

$$V_r = 0.9\,\alpha\,P_{CE}(L/h_{eff}) \quad (1)$$

$$V_{bjs1} = v_{me} A_n \quad (2)$$

$$V_{dt} = f'_{dt} A_n (L/h_{eff}) (1 + f_{ae}/f'_{dt})^{1/2} \quad (3)$$

$$V_{tc} = \alpha P_{CE} (L/h_{eff}) (1 - f_{ae}/0.7 f'_m)^{1/2} \quad (4)$$

$$K = 1/((h_{eff}^3/3E_m I_g) + (h_{eff}/A_v G_m)) \quad (5)$$

where $V_r$ and $V_{bjs}$ = shear capacity in the rocking and bed joint sliding mode, respectively, of an individual wall of width $L$, height $h$, and thickness $t$; $\alpha$ = factor equal to 0.5 for fixed-free cantilever wall, or equal to 1.0 for a fixed-fixed wall; $P_{CE}$ = expected vertical axial compressive force; $v_{me}$ = bond plus friction strength of mortar, as defined in *FEMA* 356; $A_n$ = area of net mortared/grouted section. The lower bound strength $V_{dt}$ and $V_{tc}$ corresponding to toe crushing and diagonal tension failure, $f'_{dt}$ = diagonal tension strength, assumed as vme, per *FEMA* 356; $f_{ae}$ = expected vertical axial compressive stress; $f'_{me}$ = expected masonry compressive strength; $h_{eff}$ = Wall height; $A_v$ = Shear area; $I_g$ = Moment of inertia for the gross section representing uncracked behavior; $E_m$ = Masonry elastic modulus and $G_m$ = Masonry shear modulus.

In the Table (4) in addition of strength values, predicted failure modes are also reported. The main difference between predicted and experimental is failure modes identification. Based on *FEMA* 356 almost all the modes are toe crushing while the test results indicate sliding and shear failure. The calculated lateral force displacement curves are plotted together with the measured lateral force-displacement curves in Figures (17) to (20). It is apparent that the lateral force-displacement curves given by the *FEMA* 356 are not close to that obtained from

**Table 4.** FEMA 356 prediction and observation results (strength and failure modes) .

| Wall | $V_r$ (*kN*) | $V_{bjs1}$ (*kN*) | $V_{tc}$ (*kN*) | $V_{dt}$ (*kN*) | $V_{test}$ (*kN*) | Failure Mode | |
|---|---|---|---|---|---|---|---|
| | | | | | | FEMA-356 | Experiment |
| URMW-1 | 47.8 | 54.0 | **41.3** | 72.4 | **41.8** | Toe Crushing | Slid |
| FIURMW-19 | 52.1 | 56.4 | **45.0** | 75.7 | **47.9** | Toe Crushing | Slid |
| URMW-2 | 15.4 | 26.4 | **13.3** | 35.0 | **18.3** | Toe Crushing | Diagonal Tension |
| FUURMW-18 | 16.0 | 26.9 | **13.8** | 35.7 | **12.4** | Toe Crushing | Diagonal Tension |

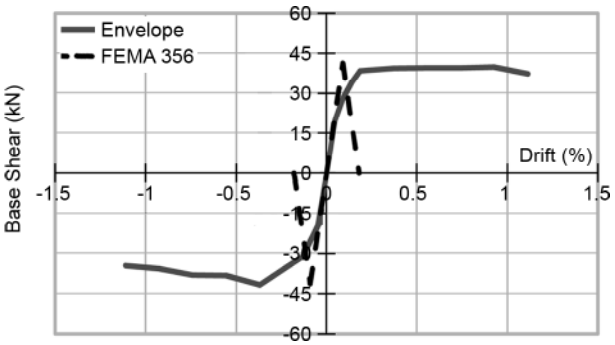


**Figure 17.** URMW-1 back bone and FEMA356 curve.

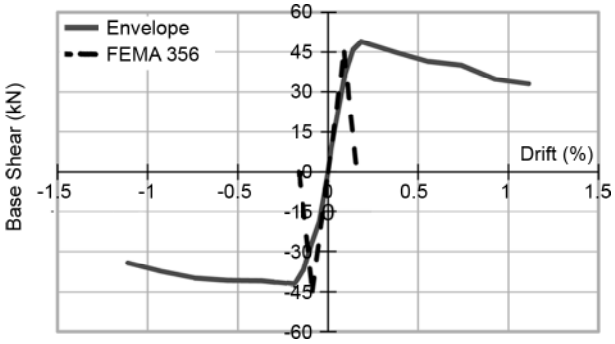


**Figure 19.** H-shaped wall back bone and FEMA356 curve.

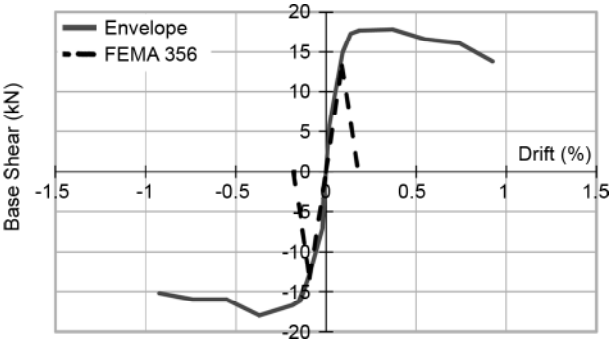


**Figure 18.** URMW-2 back bone and FEMA 356 curve.

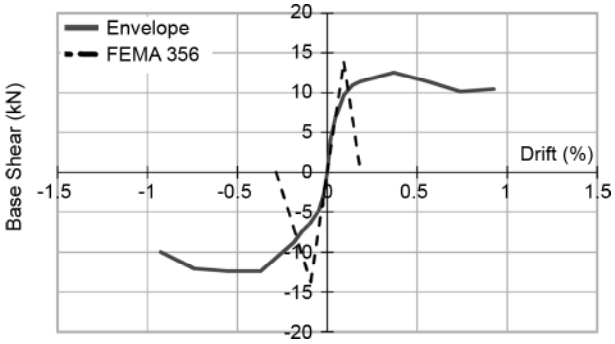


**Figure 20.** U-shaped wall back bone and FEMA 356 curve.

the tests. The deformation at maximum strength calculated was based on stiffness Eq. (5). In Force control failure mode such as Toe Crushing and Diagonal tension, for calculating the deformation of the maximum strength, it is assumed that force-drift curve increases with the slope equal to $K$ and after reaching the maximum strength, drop with the same negative slope to zero. $K$ is the lateral in plane cantilevered wall stiffness and can be calculated using Eq. (5) based on *FEMA* 356.

The results of comparison between *FEMA* 356 model and experimental results in Table (4) show that although the *FEMA* 356 could estimate the strength of the specimens with enough accuracy, the failure mode was estimated wrongly in all cases. It is important to note that, according to *FEMA* 356 approach, the minimum of lateral strength derived from four different modes (bed joint sliding, toe crushing, diagonal tension, and rocking) indicate predominate mode and corresponding strength and consequently, force-control or displacement-control behavior. When a mode is wrongly identified, although the strength may be acceptable, ductility is not proper. *FEMA* 356 equations underestimate the strength and therefore, consider some uncertainties. However, the boundary conditions (in this case the flange walls) were not adequately accounted for prediction of the wall strength. The same results are reported by other researchers [10, 11, 14, 15].

## 6. Analytical Model to Investigate the Flange Effects

Many researches have been previously presented on in-plane *URM* wall response, but it has been identified in the literature that codified equations for assessing the strength and displacement capacity of walls are overly conservative, particularly where assessing *URM* walls with flanges (return walls) at either or both ends. On the other hand, the existing model was developed for walls with a single flange on the in-plane wall (*L*-shaped wall). Therefore, it is reasonable to develop a comprehensive model to capture flange wall at both ends such as *H* or *U* sections. In this case, the shear stress distribution is different from *L*-shaped or rectangular walls. The main assumptions adopted by this model are the same provided by Yi et al [11, 29] as follows:

1. The external forces applied at the top of the wall cause cracking of some portion of the top section. The effective section at the top of the wall is defined as the un-cracked portion of the wall. Similar assumptions are used at the bottom.
2. The effective wall is defined by linearly connecting the top and bottom effective sections to the original wall boundaries at the points with a cracking moment of $M_{cr}$.
3. The axial stress normal to the bed joint, $\sigma_n$, varies linearly across the effective section.
4. The shear stress is uniformly distributed over each effective section.
5. Although the response of a non-rectangular section wall is not purely in-plane, possible torsional behavior is ignored. In general, the resultants of external forces do not necessarily go through the shear center of a non-rectangular section wall, and thus, they introduce torsion in the wall. However, since in most cases walls are laterally supported by floor systems, significant torsional deformation is typically restrained. As a result, for simplicity, it is assumed that external lateral forces are applied at the shear center of the un-cracked non-rectangular wall section and are parallel to the in-plane wall.
6. The effective length of the flange, $L_f$, can be calculated by using the method specified in the codes
7. The joint between the in-plane wall and the flange is assumed strong enough to ensure full composite action (strain compatibility) between the two walls.
8. To calculate the principal tensile stress at the inflection point of the wall for the diagonal tension limit state, a modified beam theory is employed, which considers the non-uniform shear stress distribution. For calculations related to the bed joint sliding limit state, the shear stress is assumed to be plastic and uniformly distributed.
9. To simplify the problem, masonry bed joint tensile strength is assumed to be zero.

Based on aforementioned assumption and equilibrium equations, the flange effect on the lateral strengths of *H* or *U* section walls corresponding to the four primary failure modes was developed and adopted for cantilever walls. A typical *H*-shaped *URM* wall and external applied forces are illustrated in Figures (21) and (22).

$V$ is the applied shear force; $P_t$ and $P_b$ are the compressive axial forces applied at the top and the bottom of the wall, respectively; $M_t$ and $M_b$ are the moments applied at the top and the bottom of the wall about the inertia center of the wall section, respectively; $W$ is the self weight of the in-plane wall; and $W_f$ is the self weight of the flange. The equilibrium equations give:

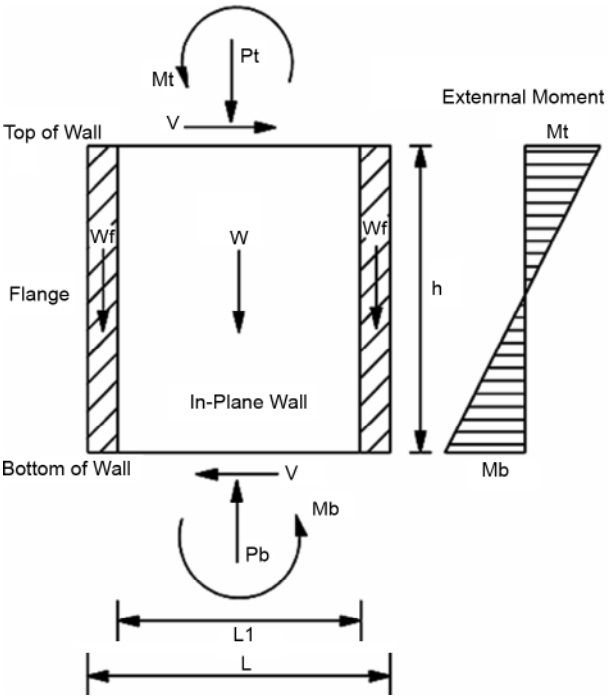


**Figure 21.** External applied forces on a H section URM walls.

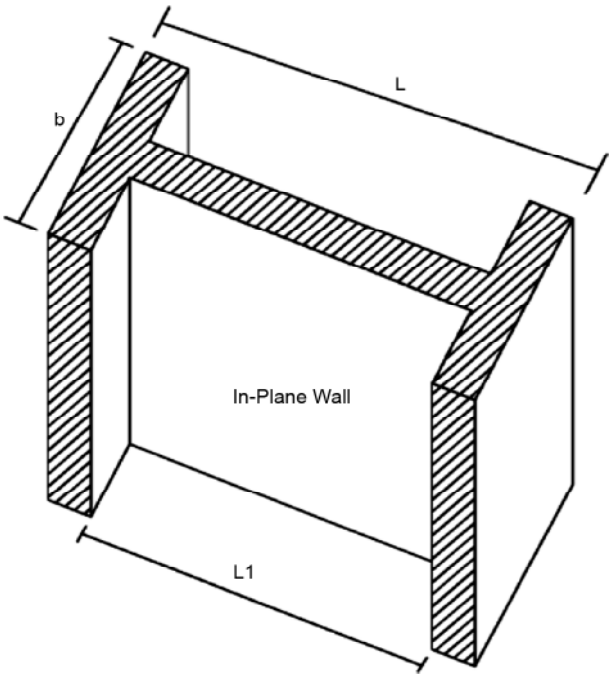


**Figure 22.** A typical URM Wall with flanges.

$$P_b = P_t + W + W_f \quad (6)$$

$$V.\ h = M_t + M_b \quad (7)$$

To simplify the problem responses of a cantilever *URM* wall are discussed in the following section. Note that in this case, although the in-plane rotation at top of the wall is not restrained ($M_t = 0$), due to lateral constraint of floor diaphragm, out-of-plane rotation at the top of the wall is restrained and can be ignored. In this case:

$$V.\ h = M_b \quad (8)$$

A rocking failure is characterized by large flexural cracks at the bottom and the top of the wall. As the displacement increases, the wall deforms and rotates about the compressive toe. When force reversals occur, the flexural cracks close and the wall behaves as an un-cracked wall until the flexural cracks open in the other direction. Internal shear stress on an *H* section *URM* walls in flexural crack mode is shown in Figure (23). In Figure (23), $\sigma_{n\,max}$ is the maximum compressive stress at the compression area; $\sigma_n$ is the compressive stress; $f_t$ is the masonry tension stress that was neglected based on assumption. The vertical stress distribution and the effective length at the bottom of the nonrectangular

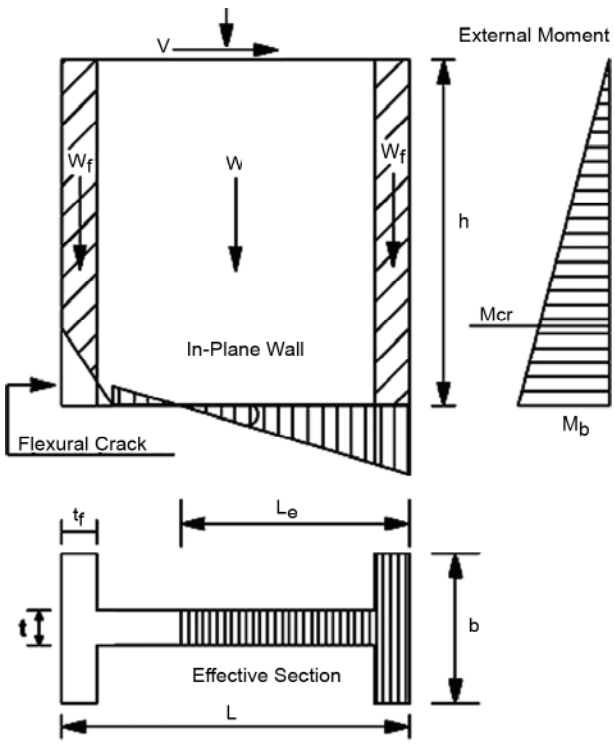


**Figure 23.** Internal shear stress on an H section URM walls in flexural.

section *URM* wall can be calculated based on the equilibrium equations and the linear vertical stress distribution assumption.

In this case, taking the bottom section and assuming that the effective length $L_e$ is less than the length of the in-plane wall, gives the lateral strength of the wall in terms of vertical force and the effective length at the bottom of the wall:

$$V_r = \frac{P_b}{h}\frac{\frac{1}{2}L_t L_e - \frac{1}{3}L_e^2 t + (L - t_f)A_f(1 - \frac{t_f}{2L_e})}{L_{eb}t + 2A_f(1 - \frac{t_f}{2L_e})} \quad (9)$$

Toe crushing occurs when the maximum compressive stress at the compression toe equals the maximum compressive strength of masonry.

$$V_{tc} = \frac{\beta f_m}{2h} \times \left[\frac{L_{etc}^2 t_w}{6} + L_{etc}t_w(L - L_e) + A_f(1 - \frac{t_f}{2L_{etc}})(L - t_f)\right] \quad (10)$$

Where, $\sigma_{n\,max}$ is the maximum compressive stress; $f_m$ is the compressive strength of masonry; and $\beta$ is a factor accounting for the nonlinear vertical stress distribution, with a value equal to 1.3. Toe crushing is the upper limit for the rocking/flexural cracking behavior [29].

### 6.1. Bed-Joint Sliding

Due to the formation of tensile horizontal crack in the bed joints, (flexural crack) subjected to reversed seismic action, potential sliding planes can form along the cracked bed joints. This failure mode is possible for low levels of vertical load and/ or low friction coefficients [4]. For calculations related to the bed joint sliding limit state, the shear stress is assumed to be plastic and uniformly distributed. In this case, by using Mohre-Colomb equation for an un-cracked or partial cracked bed joint surface, the bed joint sliding strength is determined by:

$$V_{slid} = \mu P_b + (A_f + L_e t)\tau_0 \quad (11)$$

Note that the bed-joint shear strength decreases with decreasing effective lengths at the base of the wall (as indicated in Eq. (11)), while the rocking lateral strength increases (as indicated in Eq. (9)). The bed joint sliding occurs when the bed joint sliding strength reduces to the rocking strength with the decreasing effective length.

### 6.2. Diagonal Tension

A diagonal tension failure is assumed to occur where the maximum principal tensile stress is equal to the diagonal tensile strength of masonry, see Figure (24).

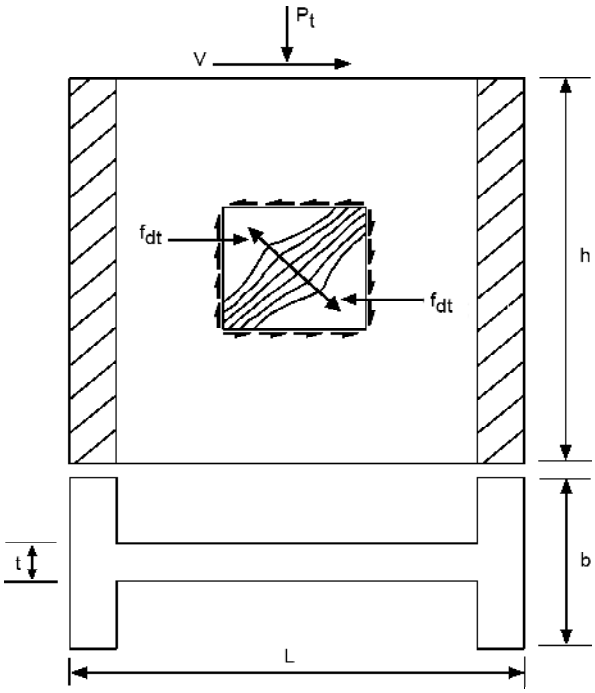


**Figure 24.** Shear strength of a wall and diagonal tension strength of masonry.

In this case:

$$\sigma_1 = f_d^t \quad (12)$$

Where, $\sigma_1$ is the maximum principle tensile stress, and $f_d^t$ is the diagonal tensile strength of masonry and calculated by using the following stress transformation equation:

$$\sigma_1 = \sqrt{\left(\frac{\sigma_{avg}}{2}\right)^2 + \left(\frac{\tau_d}{\varsigma}\right)^2} - \frac{\sigma_{avg}}{2} \quad (13)$$

Where, $\zeta$ is a factor that accounts for the erroneous shear stress distribution assumption given by beam theory, whose value varies between 1 and 1.5 depending on the aspect ratio of the wall. For slender walls ($h/L > 2$), $\zeta$ is taken as 1.5, for squat walls ($h/L < 0.5$), $\zeta$ is equal to 1.0. $\sigma_{avg}$ is the average vertical compressive stress at the midheight of wall; and $\tau_d$ is the maximum shear stress at neutral axes of wall section calculated based on a modified beam theory. It is important to note that in cantilever

walls, a combined flexural and shear stress is altered maximum principle tensile stress and consequently, resultant crack pattern, while experimental evidence as showed in Figures (13) and (14) have shown diagonal cracking pattern. Therefore, in current research, the same failure criteria that presented in Eq. (13) is used and flexural stress effects are ignored.

$$\tau_{d\,max} = \frac{3V}{2t}\frac{bL^2 - bL_1^2 + tL_1^2}{bL^3 - bL_1^3 + tL_1^3} \tag{14}$$

The maximum diagonal tension strength of a *URM* wall can be calculated by substituting Eq. (14) into Eq. (13), and the results are shown in Eq. (15):

$$V_{dt} = \frac{2_t}{3\xi}\, f_d^t \sqrt{\left(1 + \frac{\sigma_{avg}}{f_d^t}\right)^2}\, \frac{bL^3 - bL_1^3 + t_w L_1^3}{bL^2 - bL_1^2 + t_w L_1^2} \tag{15}$$

The parameters have previously defined.

## 7. Deformation and Mixed Failure Mode

Calculation of deformation and determination of mixed failure modes for a flanged wall follow the same procedure as that for a rectangular section that proposed by Yi et al [27]. A mixed failure mode of the wall is estimated by calculating the wall's internal stresses and by checking the stresses with the failure criteria. If diagonal tension failure occurs, the tangential stiffness of the wall is assigned as a negative ratio (-0.02) of its initial lateral stiffness. Assuming the lateral deformation of the wall induced by its axial deformation can be ignored, the lateral deformation of the wall is then determined by its flexural deformation and shear deformation, which can be calculated by:

$$\Delta = \frac{V_r}{K} \tag{16}$$

Where, $\Delta$ is the lateral deformation of the wall; and $K$ is the lateral stiffness of the wall, which is dependent on the dimensions, boundary conditions, and elastic modulus of the wall. For an initial elastic *URM* wall, $K$ can be calculated as:

$$K = \frac{1}{\left[\frac{4\gamma h^3}{Et L_e^3} + \frac{h}{G L_e t}\right]} \tag{17}$$

Where, $\gamma$ is a coefficient that describes the boundary conditions of the wall ($\gamma$ is equal to 1.0 for fixed-fixed end conditions, and 0.5 for cantilever end conditions); $E$ is the elastic modulus of masonry; and $G$ is the shear modulus of masonry, which is taken as $0.4E$. After the *URM* wall experiences a loss of section, the lateral stiffness of the effective *URM* wall calculated based on the new $L_e$ (effective length).

## 8. Investigate the Flange Effects by Analytical Models

An effective wall model used to determine the force displacement behavior of four walls have been reported in this paper. A nonlinear pushover program was developed to numerically simulate the response of walls.

In the *URMW*-1, Flexural cracking was observed in the bed joint at the base of the wall at about 0.05% drift. The failure modes observed for this specimen were classified as flexural cracking degrading to sliding at a drift of 0.5%. The maximum strength for the specimen was 41.7*kN*. The compressive strength of masonry was taken as 3.24*MPa* and the initial elastic modulus was taken as 486*MPa* based on material test results. Using *NZSEE* guidelines [31], the mortar in walls was classified as poor-quality mortar, with values of 0.2 and 0.6 for $c$ (cohesion) and $\mu$ (coefficient of friction) respectively. The shear factor $\zeta$ was assumed to be 1.0 because the aspect ratio ($h/L$) of this wall was 0.5. The effective pier model predicted the flexural crack at a drift of 0.55% and a lateral force of 43.2*kN*. Then the model predicted bed-joint sliding at the base of the wall.

In the *H*-shaped wall, flexural cracking was observed in the bed joint at the base of the wall. The failure modes observed were classified as flexural cracking degrading to sliding at a drift of 0.15%. The proposed model predicted the flexural crack at a drift of 0.16 % and a lateral force of 49.5*kN*. Then the model predicted bed-joint sliding at the base of the wall.

In the *URMW*-2, the specimen behavior was classified as flexural cracking degrading to diagonal tension cracking with a peak load of 18.3*kN*. The compressive strength factor $\beta$ was assumed to be 1.28, and the diagonal tension strength was taken as 0.08*MPa*. The effective pier model predicted that the flexural crack degrading to diagonal tension with a maximum strength of 18.8*kN*. The calculated maximum strength was closer to the measured value.

In the *U*-shaped wall the specimen behavior was classified as flexural cracking degrading to diagonal tension cracking with a peak load of 12.4*kN*. The proposed model predicted the flexural crack then diagonal tension failure with a lateral force of 14.6*kN*. The calculated lateral force displacement curves are plotted together with the measured lateral force-displacement curves in Figures (25) to (28). It is apparent that the lateral force-displacement curves given by the analysis are close to that obtained from the tests.

## 9. Conclusions

The influence of flanges (return walls) on in-plane lateral behavior of unreinforced masonry (*URM*) walls with weak shear strength was studied. The study included cyclic load test on four wall specimens with aspect ratios of 0.5 and 0.7, two with flanges of *H* and *U* shapes, and two others without flanges. An existing analytical model has been developed to predict the response of flanged *URM* walls. It is important to note that regarding to limit flanged wall experimental tests, the developed results on experiments and analytical approach should be considered primary and needs more investigation. Regarding the current research scope, the results showed:

1. The tests showed an increase in strength of the *H*-shaped wall with less damage relative to the reference rectangular wall.
2. A significant loss of strength is observed for the *U*-shaped wall caused by out-of-plane torsional effect relative to the reference wall.
3. Both flanged walls indicate almost similar initial stiffness, deformation capacity, and mode of failure in comparison to the reference walls.
4. It was found that the existing simplified predictive techniques do not accurately take into account the effects of boundary conditions, in particular, the influence of perpendicular walls, to the failure mode of in-plane loaded walls.
5. The proposed model was used to verify against *H*-and *U*-shaped walls with a high level of correlation.
6. It is recommended that in analysis of flanged *URM* walls, especially when determining strength, displacement capacity, or failure mode, the influence of flanges should explicitly be considered.

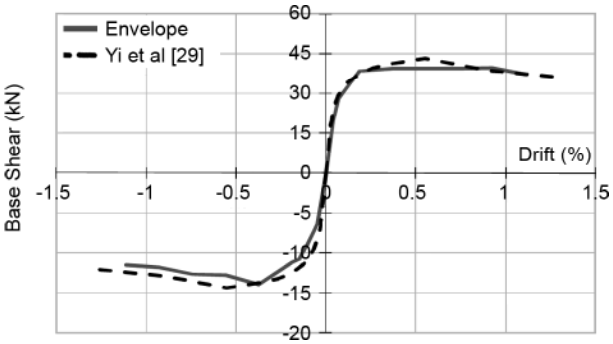


**Figure 25.** URMW-1 experimental curve and predicted analytical curve.

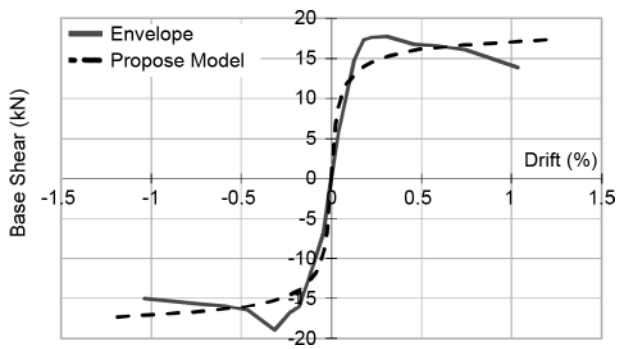


**Figure 26.** URMW-2 experimental curve and predicted analytical curve.

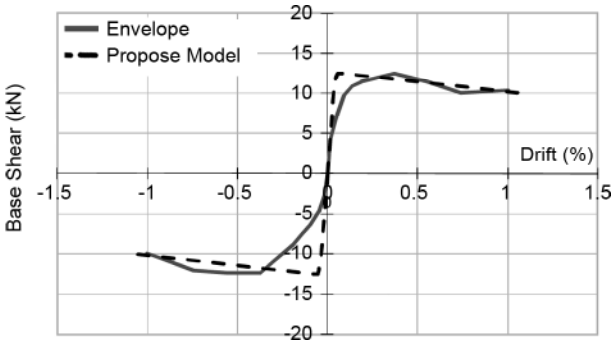


**Figure 27.** URMW-1 experimental curve and predicted analytical curve.

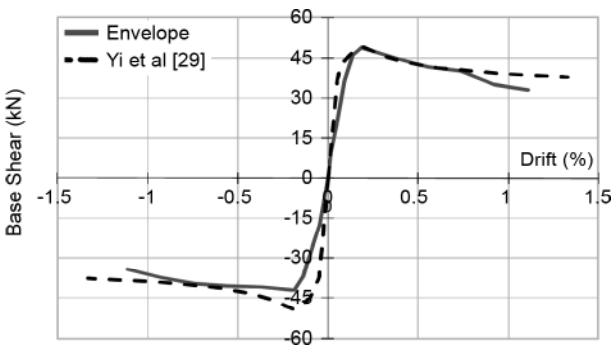


**Figure 28.** U-shaped wall experimental backbone and predicted analytical curve.

**Acknowledgments**

Test program of the specimens is supported by Tehran Disaster Mitigation and Management Organization, under agreement 190/8090, which is gratefully appreciated.

**References**

1. Abrams, D. P. (1997). "Response of Unreinforced Masonry Buildings", *Journal of Earthquake Engineering*, **1**(1), 257-273.

2. Abrams, D.P. and Shah, N. (1992). "Cyclic Load Testing of Unreinforced Masonry Walls", College of Engineering, University of Illinois at Urbana, Advanced Construction Technology Center Report, No. 92-26-10.

3. Anthoine, A., Magonette, G., and Magenes, G. (1995). "Shear-Compression Testing and Analysis of Brick Masonry Walls", *Proceedings of the 10th European Conference on Earthquake Engineering, Duma*, The Netherlands.

4. Magenes, G. and Calvi, M. (1997). "In-Plane Seismic Response of Brick Masonry Walls", *Journal of Earthquake Engineering and Structural Dynamics*, **26**.

5. Manzouri, T., Shing, P.B., Amadei, B., Schuller, M., and Atkinson, R. (1995). "Repair and Retrofit of Unreinforced Masonry Walls: Experimental Evaluation and Finite Element Analysis", Department of Civil, Environmental and Architectural Engineering, University of Colorado: Boulder, Colorado, Report CU/SR-95/2.

6. Moon, F.L., Yi, T., Leon, R.T., and Kahn, L.F. (2007). "Testing of a Full-Scale Unreinforced Masonry Building Following Seismic Strengthening", *Journal of Structural Engineering*, **133**(9), 1215-1226.

7. Yi, T. (2004). "Experimental Investigation and Numerical Simulation of an Unreinforced Masonry Structure with Flexible Diaphragms", Ph.D. Thesis, Georgia Institute of Technology, Atlanta, GA.

8. Applied Technology Council (ATC) (2000). "Prestandard and Commentary for the Seismic Rehabilitation of Buildings", Publication No. 356, Federal Emergency Management Agency, Washington, D.C. (FEMA-356).

9. Moon, F.L., Yi, T., Leon, R.T., and Kahn, L.F., (2006). "Recommendations for Seismic Evaluation and Retrofit of Low-Rise URM Structures", *Journal of Structural Engineering*, **132**(5), 663-672.

10. Yi, T., Moon, F.L., Leon, R.T., and Kahn, L.F. (2006). "Quasi- Static Tests of a Two-Story Unreinforced Masonry Building with Flexible Diaphragms", *Journal of Structural Engineering*, **132**(5), 643-652.

11. Yi, T., Moon, F.L., Leon, R.T., and Kahn, L.F. (2008). "Flange Effects on the Nonlinear Behavior of URM Walls", *The Masonry Society Journal*, **26**(2), 31-42.

12. Franklin, S., Lynch, J., and Abrams, D.P. (2001). "Performance of Rehabilitated URM Shear Walls: Flexural Behavior of Walls", Department of Civil Engineering, University of Illinois at Urbana-Champaign Urbana, Illinois.

13. Paquette, J. and Bruneau, M. (2003). "Pseudo-Dynamic Testing of Unreinforced Masonry Buildings with Flexible Diaphragm", *Journal of Structural Engineering, ASCE*, **129**(6), 708-716.

14. Russell A.P. and Ingham, J.M. (2010). "The Influence of Flanges on the In-Plane Seismic Performance of URM Walls in New Zealand Buildings", *NZSEE Conference*.

15. Russell, A.P. (2010). "Characterization and Seismic Assessment of Unreinforced Masonry Buildings", PhD Thesis, Civil and Environmental Engineering Dep., University of Auckland, New Zealand.

16. Moon, F., Yi, T., Leon, R.T., and Kahn, L.F. (2007). "Full-Scale Testing of a URM Structure Following Seismic Retrofit", *Journal of Structural Engineering, ASCE*, in Review.

17. Moon, F. L. (2004). "Seismic Strengthening of Low-Rise Unreinforced Masonry Structures with Flexible Diaphragms", Ph.D. Thesis, Georgia Institute of Technology, Atlanta, GA.18.

18. Masonry Standards Joint Committee (MSJC), (1995). "Building Code Requirements for

Masonry Structures", (ACI 530-05/ ASCE 5-05/ TMS 402-05), American Concrete Institute; Structural Engineering Institute of the American Society of Civil Engineers; The Masonry Society, Boulder CO, 220p.

19. European Committee for Standardization, Euro Code 6 (1995). "Design of Masonry Structures, Part I-1: General Rules for Buildings-Rules for Reinforced and Unreinforced Masonry".

20. ASTM (2004a). "Standard Test Method for Compressive Strength of Hydraulic Cement Mortars (Using 2-in. or [50-mm] Cube Specimens)", ASTM C 109/C 109M-2. ASTM International, USA.

21. ASTM (2003). "Standard Test Method for Sampling and Testing Brick and Structural Clay Tile", ASTM C 67-03a, ASTM International, USA.

22. ASTM (2007a). "Standard Test Method for Compressive Strength of Masonry Prisms", ASTM C 1314-07, ASTM International, USA.

23. Bruneau, M. (1994b). "State-of-the-Art Report on Seismic Performance of Unreinforced Masonry Buildings", *Journal of Structural Engineering*, **120**(1), 230-251..

24 Gu, X.L., Ouyang, Y., Zhang, W.P., and Ye, F.F., (2003). "Seismic Behavior of Masonry Structural Walls Strengthened with CFRP Plates", In Tan, K.H., Editor, FRPRCS-6, 1259-1268, Singapore.

25. Marcari, G., Manfredi, G., and Pecce, M. (2003). Experimental Behavior of Masonry Panels Strengthened with FRP Sheets", In Tan, K.H., Editor, FRPRCS-6, 1209-1218, Singapore, World Scientific Publishing Company.

26. Santa Maria, H., Alcaino, P., and Luders, C. (2006). "Experimental Response of Masonry Walls Externally Reinforced with Carbon Fibre Fabrics", *In Proc., 8th US National Conference on Earthquake Engineering*, San Francisco, California.

27. Derakhshan, H. (2011). "Seismic Assessment of Out-of-Plane Loaded Unreinforced Masonry Walls", PhD Thesis, Civil and Environmental Engineering Department, University of Auckland, New Zealand.

28. Griffith, M.C., Magenes, G., Melis, G., and Picchi, L. (2003). "Evaluation of Out-of-Plane Stability of Unreinforced Masonry Walls Subjected to Seismic Excitation", *Journal of Earthquake Engineering*, 7(SPEC. 1), 141-169.

29. Yi, T., Moon, F.L., Leon, R.T., and Kahn, L.F. (2005). "Effective Wall Model for the Nonlinear In-Plane Analysis of Individual URM Walls", *The Masonry Society Journal*, **23**(1), 21-35.

30. Magenes, G. and Della Fontana, A. (1998). "Simplified Non-Linear Seismic Analysis of Masonry Buildings", *5th International Masonry Conf., Proc. of the British Masonry Society.*

31. New Zealand Society for Earthquake Engineering (2006). "Assessment and Improvement of the Structural Performance of Buildings in Earthquake", Recommendations of a NZSEE Study Group on Earthquake Risk Buildings.